

FERROELECTRIC CERAMICS WITH HIGH PERMITIVITY FOR DIELECTRIC CAPACITOR APPLICATION

By Samrawit Daniela Hailu

Third Year Project (Mech) May 2023

Supervisor: Prof Haixue Yun

SCHOOL OF ENGINEERING AND MATERIALS SCIENCE

THIRD YEAR PROJECT

DEN318

MAY 2023

DECLARATION


This report entitled

FERROELECTRIC CERAMICS WITH HIGH PERMITIVITY FOR DIELECTRIC
CAPACITOR APPLICATION

Was composed by me and is based on my own work. Where the work of the others has been used, it is fully acknowledged in the text and in captions to table illustrations. This report has not been submitted for any other qualification.

Name Samrawit Daniela Hailu

Signed

.....

Date02/05/2023.....

Abstract

This report investigated the ferroelectric properties of two compositions of strontium and hafnium doped barium titanate, $\text{Ba}_{0.72}\text{Sr}_{0.28}\text{Ti}_{0.89}\text{Hf}_{0.11}\text{O}_3$ and $\text{Ba}_{0.70}\text{Sr}_{0.30}\text{Ti}_{0.89}\text{Hf}_{0.11}\text{O}_3$. The main aim of this report is to develop ferroelectric ceramics with permittivity $>10,000$ for dielectric capacitor application. The conventional solid-state method was used for synthesis. The crystalline structure of sintered ceramics is examined by X-ray diffraction, resulting in data supporting the false presence of a cubic phase structure. Ceramics' density is determined using the Archimedes method. The temperature dependence of the dielectric permittivity (P-E) and current-electric field (I-E) hysteresis loops are recorded using the Radiant ferroelectric workstation, which demonstrated ferroelectric behaviour and domain switching in both compositions. It has been found that $\text{Ba}_{0.72}\text{Sr}_{0.28}\text{Ti}_{0.89}\text{Hf}_{0.11}\text{O}_3$ has a permittivity of 5,500 and $\text{Ba}_{0.70}\text{Sr}_{0.30}\text{Ti}_{0.89}\text{Hf}_{0.11}\text{O}_3$ has a permittivity of 12,000, therefore the second composition achieves the aim. The temperature dependence, frequency dependence, structure, defects, and grain size are also discussed.

Contents

Abstract

1.Introduction and Literature Review.....	1-5
2. Materials.....	5-6
3. Method.....	6
4.Results and Discussion.....	7-13
4.1 P-E and I-E hysteresis loop analysis.....	10
4.2 XDR Analysis.....	10-11
4.3 Frequency Dependence.....	11
4.4 Defect Analysis.....	11-12
4.5 Grain Size Analysis.....	12
4.6 Temperature Dependence.....	13
5. Conclusion.....	13
6. References.....	14-17

1. Literature Review and Introduction

The origin of ferroelectricity can be dated back to 1924 by W.F.G. Swann where he began the study of the relation of ferromagnetism and Rochelle salts [1], Sodium potassium tartrate tetrahydrate, which was used for its moderate purgative medicinal effects for over 200 years [2]. Ferroelectricity describes the phenomenon of spontaneous polarisation below the Curie temperature (T_c) and the ability of the potential direction change of the dipoles due to the application of an electrical field. [3] The polarization-electric field (P-E) curve develops hysteresis loops as a result of this reversible switching. Ferroelectric materials are desirable for capacitor applications because they have a high dielectric constant. [4]

Dielectric capacitors function by the lack of movement of electrons, acting as an insulator. As the nuclei move, there is an increased positive charge on one side and an increased negative charge on the other, forming a dipole. When there is an electrical field present, the electrons will exert force against the field. Polarisation is the name given to this process. Therefore, for applications involving dielectric capacitors, the material's capacity for this kind of polarisation is crucial. [5]

An indicator of a material's capacity to store electrical energy is its dielectric constant (κ). It is described as the difference in capacitance between a capacitor with a substance as the dielectric and one with a vacuum as the dielectric. The formula for the dielectric constant is:

$$Eq. 1 \quad \kappa = \epsilon_r = \frac{\epsilon_m}{\epsilon_0}$$

where the dielectric constant is defined by the relative permittivity (ϵ_r) which is directly proportional to the permittivity of the material (ϵ_m) over the permittivity of a vacuum (ϵ_0). The dielectric constant of ferroelectric materials is high and can be in the range of a few hundred to several thousand.[6]

The idea that materials with a single crystallite structure have a specific chemical composition consisting of ions, or atoms with a negative and positive charge, helps simplify the structure of ferroelectric materials. The smallest repeating unit is referred to as a unit cell, and these atoms have precise locations in relation to one another. The piezoelectric potential, which in turn affects its characteristics, depends on the symmetry of these unit cells. The unit's core has a number of symmetrical components, including the symmetry centre, rotational axes, and mirror planes, however it is also conceivable for it to combine many of these. Triclinic, monoclinic, orthorhombic, tetragonal, rhombohedral, hexagonal, and cubic crystal systems are the seven fundamental crystal systems, which are listed in ascending symmetry. [7] The polar axes of ferroelectric materials also have a random orientation after synthesis and sintering; however, because these polar axes may be

changed by an electric field, an overall orientation is kept after polarisation. Beyond a certain temperature, known as the Curie temperature (T_c), ferroelectric ceramic materials do not exhibit ferroelectric behaviour. Below that temperature, the polar axis undergoes a ferroelectric transition that results in spontaneous polarisation. [8]

Polycrystalline ferroelectric ceramics are composed of large number of randomly oriented grains. Each grain is made up of several domains, each of which is made up of a variety of unit cells. Domain switching is the reorientation of ferroelectric ceramics' existing domains in response to external loads like electric fields and stress. At higher temperatures, the cells exhibit cubic symmetry, which renders them nonpolar since the centres of the positive and negative ionic charges coincide. However, at temperatures below the Curie temperature (material-specific), a dipole moment appears as a result of a separation between the centres of positive and negative ionic charges. The term polarisation refers to a cell's dipole moment per unit volume. Each cell in a domain has the same polarisation vector.

In the case of Barium Titanate (BaTiO_3), it has a tetragonal structure at room temperature, however at the Curie temperature and above it transitions to a cubic one as Shown in Figure 1.

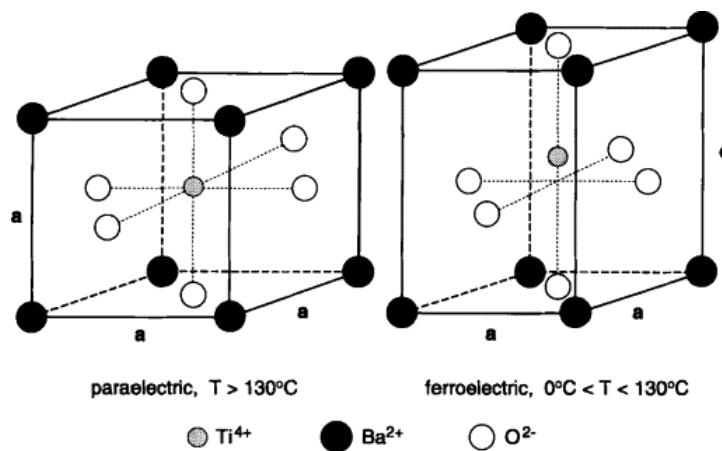


Figure 1: Demonstrating the temperature structure of barium titanate in its structural cubic phase (left) and its tetragonal phase (right) [9]

This is further confirmed by the observation that temperature-dependent aberrations from cubic symmetry accompany phase transitions in barium titanate. As a result, cations are often displaced in relation to the oxygen octahedron along their directions. Barium titanate has a perovskite structure (10/10), and ABO_3 -type perovskite oxides like these may be adjusted by substituting certain ions in the A and/or B sites to vary their characteristics for a particular application [11,12]. Barium Titanate's (BaTiO_3) ferroelectric-paraelectric transition's nature and temperature may be changed by partially replacing either Barium ions (A-site doping) or Titanium ions (B-site doping). A-site

doping with cations that have the same valence as the barium ion changes the Curie temperature (T_c), which is 130 °C in BaTiO₃, but does not significantly extend the transition between phases. The co-off-centre displacement of Ti⁴⁺ ions in their TiO₆ octahedra, often known as the ferroelectric domains, is disrupted by the presence of the B- site, which commonly widens the transition at T_c . Titanium can be partially replaced with tin, zirconium, or hafnium, which frequently causes a drop in T_c and an increase in the maximum permittivity with dopant concentration. [13] In the cubic perovskite BaTiO₃, as previously explained, the six oxygen atoms serve as the titanium atoms' octahedral coordinates. Tetragonal BaTiO₃ exhibits ferroelectricity due to the average relative displacement of titanium along the c-axis from its centrosymmetric position in the unit cell, which leads to the creation of a permanent electric dipole. The unit cell's elongation along the c-axis and the resulting deviation of the c/a axis ratio from unity demonstrate the presence of the ferroelectric phase. [14]

Because the ferroelectric-paraelectric phase transition can be shifted to room temperature through chemical modification of BaTiO₃, its electrocaloric properties can be improved. By spreading the ferroelectric-paraelectric phase transition, it is possible to increase the electrostrictive strain and dielectric energy storage capability of ferroelectric barium titanate. You can get a high and temperature-stable permittivity by improving relaxation behaviour or laminating compositions with a very high permittivity. [15]

A material's domain motion and structure are intimately related to its ferroelectricity. At Curie temperature, barium titanate experiences a phase transition from cubic, which is the paraelectric phase, to tetragonal, which is the ferroelectric phase, as previously indicated. The microstructure is influenced by the sintering process as well as the presence of additives, which results in a particular kind and configuration of domains. BaTiO₃ ceramics exhibit stable and constant ferroelectric behaviour due to their uniform, fine-grained microstructure with a single domain structure. [16] Defects have an impact on the residual polarisation, domain wall motion, dielectric constant, and leakage current of ferroelectric materials. The most mobile and prevalent defects in perovskite ferroelectrics are assumed to be oxygen vacancies, which are also the most numerous. [17]

In research conducted by Wu et al., the impedance semicircle of grain boundary phases clearly grew when the Sr/Ba ratio rose. It is hypothesised that grain boundary phases boosted the ceramics' relaxing process. The observed dielectric relaxation behaviours corresponding to the grain boundary phases were connected with the thermally triggered movements of defects because the impedance semicircle shrank as measurement temperature increased. The microstructures, energy storage

capabilities, and dielectric relaxation behaviours of strontium doped barium titanate ceramics were all greatly influenced by the Sr/Ba ratio. [18]

Local fields and polarisation patterns in ferroelectrics can be changed by defect-induced lattice deformations. [19] Atomic relaxations surrounding vacancies are boosted by hole capture or electron ionisation, and in some configurations, this results in the formation of an antiphase polarisation. Such antiphase polarisations caused by vacancies can be crucial to domain pinning and polarisation deterioration. Atomic configurations in perovskites' ferroelectric phase exhibit displacive behaviour, and it has been hypothesised that the correlation length of the polarisation is around 10–50 nm along the c axis and 1-2 nm along the a and b directions, resulting in a needle-shaped correlation volume. To balance the polarisation charges brought on by the sudden polarisation change and stabilise these domains, positively charged carriers have a tendency to gather near the tails of antiphase polarisation domains. Ageing is facilitated by the stabilisation of antiphase domains by charge trapping at defects such oxygen vacancies, which leads to a reduction in switchable polarisation. The banded structure, which predominates in a coarse-grained microstructure apart from the single domain, affects the ferroelectric properties by causing the permittivity inside the crystal to be uneven. [20]

Ferroelectric ceramics have a wide range of application as a direct result of their piezoelectric and electrostrictive properties. The four main groups are generators, motors, combined (motor/generator) and resonant devices.

Table 1: Shows the applications of ferroelectric ceramics with examples for motors, generators, combination, and resonant devices.[9]

Application type	Motors	Generator	Combination (Motor/ Generator)	Resonant Devices
Examples	<ul style="list-style-type: none"> -Actuators (macro and micro) -Camera shutters, autofocusing -Ink jet primers -Valve controllers -Pumps -Nebulizers -Ultrasonic motors -Piezoelectric fans 	<ul style="list-style-type: none"> -Hydrophones -Microphones -Phonograph Cartridges -Gas ignitors -Accelerometers -Power supplies -Photoflash actuators -Sensors -Piezoelectric pens -Impact Fuses 	<ul style="list-style-type: none"> -Sonar -Ranging transducers -Non- destructive testing (NDT) -Medical Ultrasound -Filters -Piezoelectric transformers 	<ul style="list-style-type: none"> -Ultrasonic cleaners -Ultrasonic welders -Filters (IF, SAWs) -Transformers -Delay lines

Table 1 shows the wide range of applications and the necessity of developing ferroelectric ceramics that perform optimally at working conditions.

The aim of my investigation is to develop ferroelectric ceramics with high permittivity (>10,000) at room temperature for dielectric capacitor application. This is achieved through the suppression of ferroelectric properties to allow for stability, maintaining a dielectric constant over varying conditions and establish high insulation constant, this ensures that the capacitor does not discharge over time, which can affect its performance and reliability.

To achieve this aim, two compositions of widely used ferroelectric material, Barium Titanate doped with Strontium (Sr) and Hafnium (Hf), were established $\text{Ba}_{0.72}\text{Sr}_{0.28}\text{Ti}_{0.89}\text{Hf}_{0.11}\text{O}_3$ and $\text{Ba}_{0.70}\text{Sr}_{0.30}\text{Ti}_{0.89}\text{Hf}_{0.11}\text{O}_3$. The varying Barium/Strontium ratio is considered, as well as the presence of Hafnium in altering the structure and properties of the material.

2. Materials

High purity powders of were used as raw materials to synthesise two different compositions. The mass of each required powder was calculated using Table 2 and 3 shown below. The raw materials are pre-heated at 200 °C for 24 hours.

Table 2: Calculation of the mass required powder to synthesise the composition, $Ba_{0.72}Sr_{0.28}Ti_{0.89}Hf_{0.11}O_3$, including the purity of the raw materials

$Ba_{0.72}Sr_{0.28}Ti_{0.89}Hf_{0.11}O_3$	$BaCO_3$	$SrCO_3$	HfO_2	TiO_2
n (mol)	0.72	0.28	0.11	0.89
Molar mass (g/mol)	197.34	147.63	210.49	79.866
m (g)	142.0848	41.3364	23.1539	71.08074
m/5.553 (g)	25.58703404	7.443976229	4.169620025	12.80042139
purity	99.8%	99.9%	99%	99.8%
m_{final} (g)	25.63831066	7.451427657	4.211737399	12.82607354

Table 3: Calculation of the mass of required raw powder to synthesise the composition, $Ba_{0.72}Sr_{0.28}Ti_{0.89}Hf_{0.11}O_3$, including the purity of the raw materials

$Ba_{0.70}Sr_{0.30}Ti_{0.89}Hf_{0.11}O_3$	$BaCO_3$	$SrCO_3$	HfO_2	TiO_2
n (mol)	0.7	0.3	0.11	0.89
Molar mass (g/mol)	197.34	147.63	210.49	79.866
m (g)	138.138	44.289	23.1539	71.08074
m/5.533 (g)	24.96620278	8.004518344	4.184691849	12.84669076
purity	99.8%	99.9%	99%	99.8%
m_{final} (g)	25.01623525	8.012530875	4.226961464	12.87243564

3. Method

To obtain the following compositions of Barium Titanate doped with Hafnium and Strontium, the conventional solid-state method was implemented.

In a nylon jar containing zirconia balls and ethanol, stoichiometric quantities of the raw components were ball-milled for five hours using a planetary. The slurry was dried, then calcined at 1250°C for 4 hours in a furnace, followed by a secondary ball-milling process for 5 hours to get a fine particle size to eliminate dielectric anomalies (36). After passing the powder through a 250 m sieve, 5 wt% polyvinyl alcohol (PVA) was added, and the mixture was then compressed at a pressure of 100 MPa to form discs that were 13 mm in diameter and 1-2 mm thick. To remove the binder, the pellets were heated to an internal temperature of 800 °C in air at a rate of 10 °C per minute. Based on measurements of sample density, the sintering temperature for each composition was optimised within the range of 1350 °C. Sintering was done at a 3 °C min⁻¹ heating rate with a 4-hour dwell time at the optimal temperature allowing for densification.

To evaluate the material's qualities, the sample goes through several tests. The crystalline structure of sintered ceramics is examined by X-ray diffraction (XRD, Shimadzu 7000). Ceramics' density is determined using the Archimedes method. The temperature dependence of the dielectric permittivity is obtained using an HIOKI 3532 LCR metre. The polarization-electric field (P-E) and current-electric field (I-E) hysteresis loops are recorded using the Radiant ferroelectric workstation. [21] Silver paste was then used to polish the ceramics on both sides in preparation for dielectric and hysteresis characterizations using the Sawyer Tower circuit and LCR metre, respectively. [22]

4. Results and Discussion

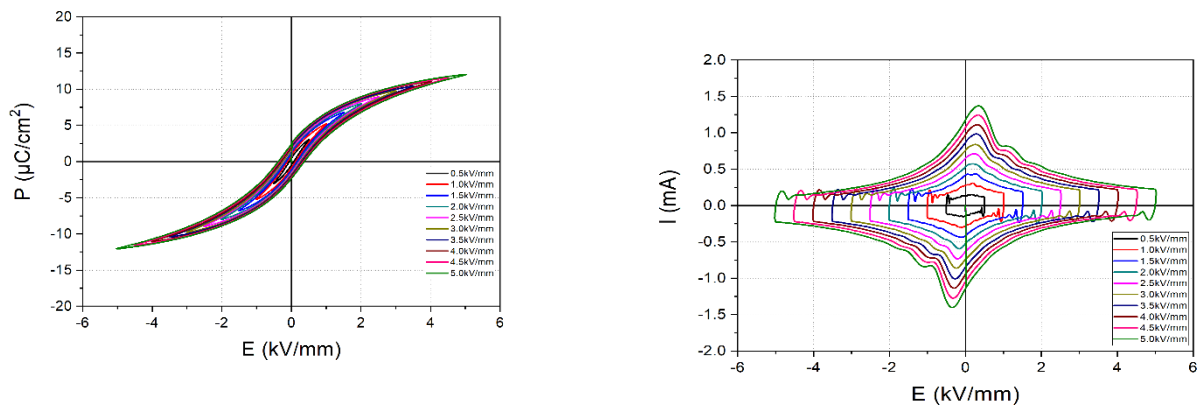


Figure 2: Shows the polarisation – electrical field hysteresis loop (left) and the current- electrical field loop (right) at different applied voltages for $\text{Ba}_{0.72}\text{Sr}_{0.28}\text{Ti}_{0.89}\text{Hf}_{0.11}\text{O}_3$

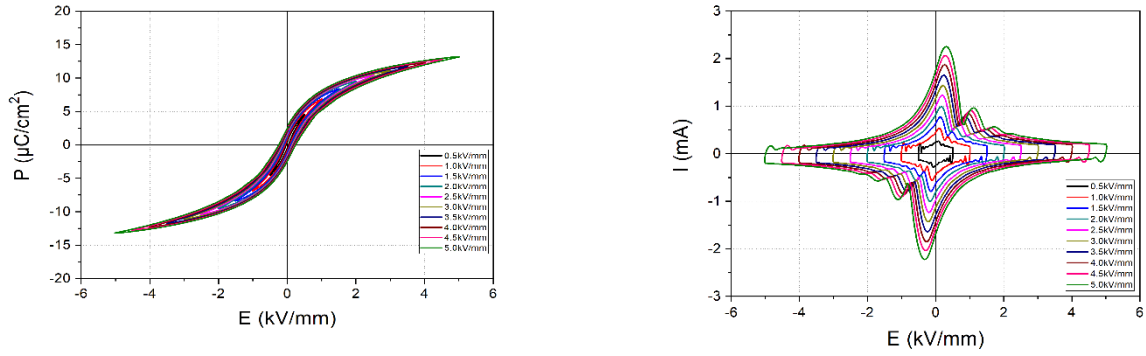


Figure 3: Shows the polarisation – electrical field hysteresis loop (left) and the current- electrical field loop (right) at different applied voltages for the composition $\text{Ba}_{0.70}\text{Sr}_{0.30}\text{Ti}_{0.89}\text{Hf}_{0.11}\text{O}_3$

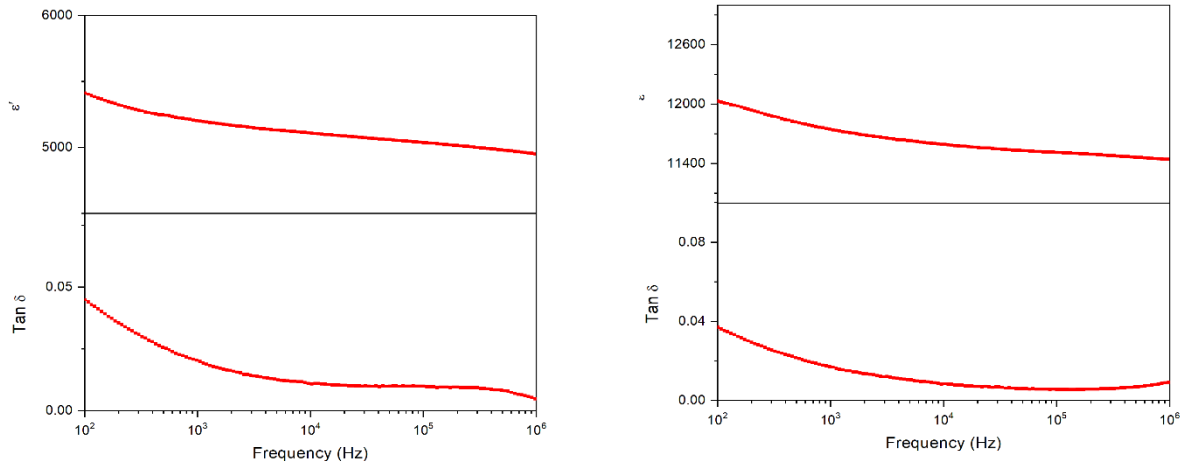


Figure 4: Illustrates the permittivity on the top and the dielectric loss on the bottom of each of composition, $\text{Ba}_{0.72}\text{Sr}_{0.28}\text{Ti}_{0.89}\text{Hf}_{0.11}\text{O}_3$ (left) and $\text{Ba}_{0.70}\text{Sr}_{0.30}\text{Ti}_{0.89}\text{Hf}_{0.11}\text{O}_3$ (right)

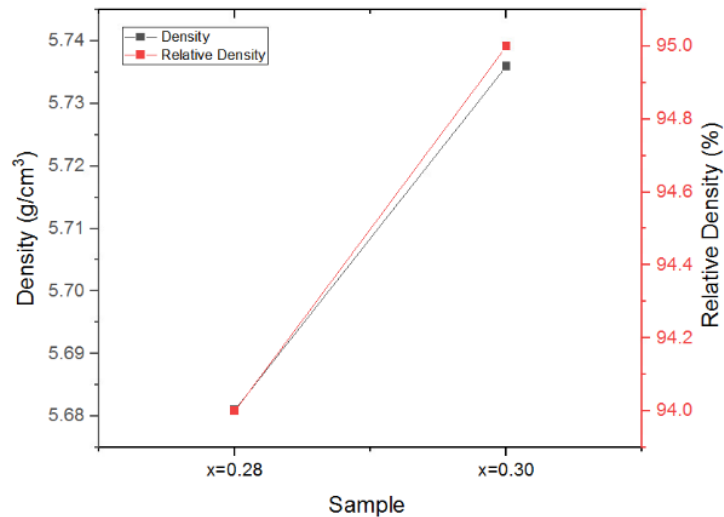


Figure 5: A comparison of the measured density versus the relative density for each sample, $x=0.28$ is $\text{Ba}_{0.72}\text{Sr}_{0.28}\text{Ti}_{0.89}\text{Hf}_{0.11}\text{O}_3$ and $x=0.30$ is $\text{Ba}_{0.70}\text{Sr}_{0.30}\text{Ti}_{0.89}\text{Hf}_{0.11}\text{O}_3$

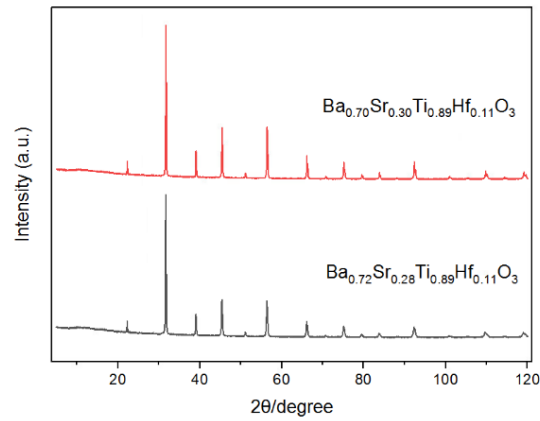


Figure 6: XRD patterns for both compositions, $Ba_{0.72}Sr_{0.28}Ti_{0.89}Hf_{0.11}O_3$ and $Ba_{0.70}Sr_{0.30}Ti_{0.89}Hf_{0.11}O_3$

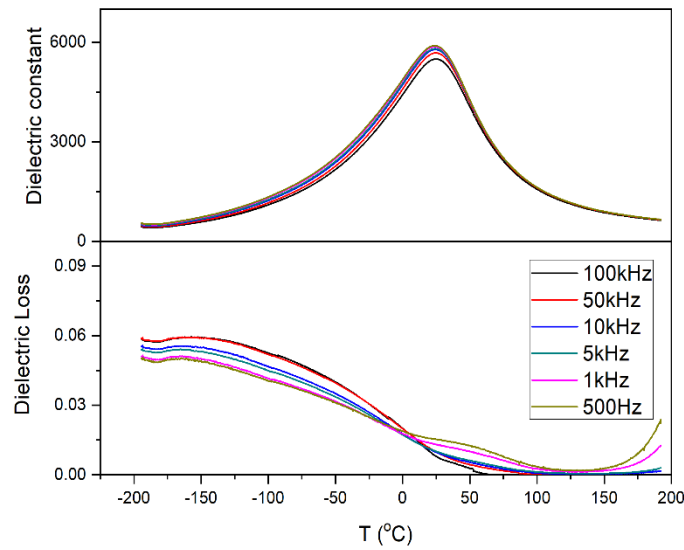


Figure 7: Temperature dependence of the dielectric constant and dielectric loss for composition $Ba_{0.72}Sr_{0.28}Ti_{0.89}Hf_{0.11}O_3$

Table 4: Shows the electric coercivity (E_C), remanent polarisation (P_R) and saturation polarisation (P_S) values obtained from the P - E hysteresis loop of compositions $Ba_{0.72}Sr_{0.28}Ti_{0.89}Hf_{0.11}O_3$ and $Ba_{0.70}Sr_{0.30}Ti_{0.89}Hf_{0.11}O_3$

Composition	E_C (kV/mm)	P_R ($\mu\text{C}/\text{cm}^2$)	P_S ($\mu\text{C}/\text{cm}^2$)
$Ba_{0.72}Sr_{0.28}Ti_{0.89}Hf_{0.11}O_3$	0.371	2.542	8.462
$Ba_{0.70}Sr_{0.30}Ti_{0.89}Hf_{0.11}O_3$	0.266	2.995	9.785

4.1 P-E and I-E hysteresis loop Analysis

When comparing the P-E hysteresis loops for the compositions it is evident that composition $Ba_{0.70}Sr_{0.30}Ti_{0.89}Hf_{0.11}O_3$ has lower ferroelectric properties as it has a lower ability to flip the polarisation between positive and negative values, an electric field is necessary, according to Table 4, as the electric coercivity is 0.371 kV/mm for composition $Ba_{0.72}Sr_{0.28}Ti_{0.89}Hf_{0.11}O_3$ and 0.226 kV/mm for composition $Ba_{0.70}Sr_{0.30}Ti_{0.89}Hf_{0.11}O_3$, demonstrates a 33% difference. Additionally, the level of polarisation that a material has after being freed from an electric field is also shown in Table 4 by the P_R value, being $2.542 \mu C/cm^2$ for composition $Ba_{0.72}Sr_{0.28}Ti_{0.89}Hf_{0.11}O_3$ and $2.995 \mu C/cm^2$ in composition $Ba_{0.70}Sr_{0.30}Ti_{0.89}Hf_{0.11}O_3$, at high electric field strengths there is a 16% difference. The maximum amount of polarisation that can be induced in the material is also greater in composition $Ba_{0.70}Sr_{0.30}Ti_{0.89}Hf_{0.11}O_3$ being $8.462 \mu C/cm^2$ and in composition $Ba_{0.72}Sr_{0.28}Ti_{0.89}Hf_{0.11}O_3$ being $9.785 \mu C/cm^2$, these values have a 15% difference. [23] The comparison of these values demonstrates that electric coercivity is most effected by the change in the barium/strontium concentration ratio in the compositions as the concentration of the other dopant, hafnium, is the same. A reason for this may be the decrease in oxygen vacancies with an increased concentration of A-site doping. Another factor to consider is the change in ionic radii after substitution, there was a net increase in the size of ions, this can cause a stronger polarisation potential due to the presence of larger ions causing more interaction between particles.

The I-E hysteresis curves in Figures 2 and 3 show a large peak which corresponds to domain switching, followed by a smaller second peak which may suggest the presence of a secondary phase. However, it is far more likely electric field induced or as a result of the presence of defects in both compositions. The intensity of both peak in Figure 2 is less than that of Figure 3, this could be due to a larger number of defects present in $Ba_{0.70}Sr_{0.30}Ti_{0.89}Hf_{0.11}O_3$ as the substitution of Sr^{2+} has given rise to an increase of domain walls and polar regions.

4.2 XDR Analysis

In Figure 6 there is an absence of small peaks, which is advantageous as it suggests that the material corresponds to a perovskite phase, which suggests the absence of secondary phase grains for both compositions. [24,25] Additionally, the XDR results in Figure 6 confirms that a cubic crystal system is maintained in both the compositions at room temperature [26]. This is shown through the peaks present at $\langle 100 \rangle$, $\langle 110 \rangle$, $\langle 111 \rangle$ domain planes, coinciding with literature [27]. Although, based on the XDR, it exhibits cubic phase peaks, the high permittivity observed in Figure 4 contradicts this.

This is because polarisation on that capacity cannot occur in the cubic phase, therefore the compositions exist in it tetragonal form.

4.3 Frequency Dependence

Figure 4 shows that for composition $Ba_{0.72}Sr_{0.28}Ti_{0.89}Hf_{0.11}O_3$ the permittivity is approximately 5,500 whereas for composition $Ba_{0.70}Sr_{0.30}Ti_{0.89}Hf_{0.11}O_3$ the permittivity is 12,000. The high permittivity for composition $Ba_{0.70}Sr_{0.30}Ti_{0.89}Hf_{0.11}O_3$ is ideal as it achieves the aim of the investigation, as it allows for a larger store of energy when voltage is applied. Additionally, the dielectric loss in composition $Ba_{0.70}Sr_{0.30}Ti_{0.89}Hf_{0.11}O_3$ is lower than that of $Ba_{0.72}Sr_{0.28}Ti_{0.89}Hf_{0.11}O_3$, demonstrating higher efficiency. Figure 2 presents the frequency dependence of dielectric constant and dielectric loss for two compositions with varying Sr/Ba ratio. In the measured frequency range, the dielectric constant of samples showed good frequency stability, as the composition $Ba_{0.72}Sr_{0.28}Ti_{0.89}Hf_{0.11}O_3$ had a decrease of approximately 500 and for composition $Ba_{0.70}Sr_{0.30}Ti_{0.89}Hf_{0.11}O_3$ it was approximately 600. In dielectrics with ion-displacement polarisation, the ion radius affects the dielectric constant. Due to Sr^{2+} lower radius compared to Ba^{2+} , the dielectric constant fell as the Sr mol percentage increased. The Sr^{2+} related polarisation was weak, which had a minor impact on the dielectric constant and contributed to its decline. Both compositions processed the paraelectric phase at room temperature, which helped to slow the dielectric loss down over time. With rising Sr contents, the grain size clearly shrank, and a uniform distribution was seen. The optimisation of microstructures is caused by a reduction in the lattice parameter and a densification of the microstructure, which is demonstrated by a reduction in dielectric loss. [28]

4.4 Defect Analysis

Defects in the structure have been caused by the hafnium and strontium doping of barium titanate; the replacement of Hf at the Ti site is creating nanoscale compositional variability as a result of the defect. Hf ions tend to increase the distance between off-centre Ti dipoles, decreasing the correlation between these dipoles in the process. The oxygen octahedra will get substituted distorted as a result of the size mismatch between the Ti and Hf ions, creating the local electric field and strain field. [29] The unstable nature of Barium Titanate can be linked to instability of valence in Ti^{+4} , however when substituting a more chemically stable ion, like Hafnium, the number of oxygen vacancies is decreased. This in turn increases the domain wall density which increases the permittivity of the material.[30] This is evident in the density data collected in Figure 5, eventhough

the difference between the measure density and relative density is negligible, it is noteworthy that composition $Ba_{0.70}Sr_{0.30}Ti_{0.89}Hf_{0.11}O_3$ has a 95% relative density while composition $Ba_{0.72}Sr_{0.28}Ti_{0.89}Hf_{0.11}O_3$ has a 94% relative density. This difference was brought on by a larger substitution of Hafnium, decreased the oxygen vacancies and increased the domain wall density and as a result the permittivity of the materials, but specifically in $Ba_{0.70}Sr_{0.30}Ti_{0.89}Hf_{0.11}O_3$. The introduction of dopants also caused defects as a result of polar regions and domain wall orientation.

4.5 Analysis of grain size

For the first time, Chaoliang et al. [31] investigated the dielectric characteristics of doped barium titanate in a bias DC field. The findings showed that ceramics with finer grains exhibit larger surface effects, mechanical stresses, and extrinsic grain boundary effects. This causes T_c to drop, the diffusion phase transition to occur more frequently, and the dielectric characteristics to worsen. [32] It has been discovered through several experimental and theoretical research that the grain size of barium titanate affects the phase-transition temperature and that the ferroelectric phase becomes unstable at ambient temperature when the particle diameter falls below a threshold level. It was discovered that as the calcination temperature rose, so did the size of the barium titanate crystallites and particles. Improvements in characteristics including ferroelectricity, piezoelectricity, relative permittivity, Curie temperature, and coercive field are significantly influenced by grain size and domain size. Dielectric and ferroelectric characteristics are reduced by big particle size. On the other hand, it has been discovered that Curie temperature rises as grain size does. The calcination temperature, sintering duration, and temperature all have a significant impact on grain size, therefore these factors were considered when determining the methodology. [33]

The dielectric constant of BT rises as the sintering temperature rises. Dielectric constant values of BT are determined for samples at a sintering temperature of 1350°C using a frequency of 1 KHz. Domains exist in the crystals of ferroelectric materials. The domain is the region in which there is uniform polarisation. As crystalline size increases, ferroelectric domains expand, and the polarisation intensifies. It suggests that BT's dielectric constant is rising. [34] It happens as a result of increased atomic diffusion and agglomeration brought on by greater sintering temperatures. There is an inverse relationship between grain size and ceramic density, where bigger grains result in denser ceramics. As a result of the higher temperatures, the bigger grain sizes that were obtained as the high temperature (1350°C) during sintering gives the agglomeration process among the particles more energy to persuade it. [35]

4.6 Temperature Dependence

Figure 7 shows how the dielectric constant varies with temperature; the composition $Ba_{0.72}Sr_{0.28}Ti_{0.89}Hf_{0.11}O_3$ dielectric peak was discovered at approximately 25°C. This shows that the temperature at which the ferroelectric-paraelectric phase transition occurs has been decreased to room temperature, and this is connected to the structure of the grain's core and shell. [36] The dielectric constant peak likewise broadens and is suppressed. The inhomogeneous distribution of Sr^{2+} and Hf^{4+} inside the crystallite structure may have led to a diffuse phase transition, which might have been the origin of this. 6,000 is the dielectric constant. The unevenness of the sample made it difficult to gather correct data from the HIOKI 3532 LCR metre, thus it's crucial to note that these results are not entirely accurate. The information was added to show how the material's dielectric peak shifted to room temperature, suppressing its ferroelectric capabilities, and allowing it to exist with greater stability.

The ions are driven by the A-site towards lower valence and the B-site towards greater valence. Thermal energy is also a factor in the site's occupancy. The ions are driven towards increased valency by increasing temperature. At a given temperature, increased oxygen partial pressure results in larger concentrations of holes and lower concentrations of electrons, which also influences the occupancy of the site. Additionally, it was discovered that dopants with larger ionic radii occupy the A-site as opposed to the B-site as evident on the compositions investigated. [37]

5. Conclusion

Overall, the introduction of Hafnium and Strontium as dopants for Barium Titanate were advantageous in achieving the aim for $Ba_{0.70}Sr_{0.30}Ti_{0.89}Hf_{0.11}O_3$ as the permittivity was greater than 10,000. However, for the second composition, $Ba_{0.72}Sr_{0.28}Ti_{0.89}Hf_{0.11}O_3$, the permittivity was less than the required value for this investigation. Furthermore, A-site doping of Strontium enabled the decrease in the Curie temperature and B-site doping allowed the widening of the T_c range, increasing the electrostrictive strain and dielectric strain capabilities. The defects caused by the domain wall and polar regions, as well as oxygen vacancies has an impact on the residual polarisation, domain wall motion, dielectric constant, and leakage current. A small grain size decreased the T_c , but increased density and the dielectric constant. The use of $Ba_{0.70}Sr_{0.30}Ti_{0.89}Hf_{0.11}O_3$ for dielectric capacitor application is recommended, dependent on further research on the properties in real life working conditions and requirement

6. References

1. Cross L, Newnham R. Huh-Technology Ceramics-Past, Present, and Future. [cited 2023 Apr 23];111. Available from: <https://citeseerx.ist.psu.edu/document?repid=rep1&type=pdf&doi=833a10adede1ed039de52f3fa0507184f2d43bc7>
2. Kwei GH, Lawson AC, Simon, Cheong SW. Structures of the ferroelectric phases of barium titanate. *The Journal of Physical Chemistry*. 1993 Jan 1;97(10):2368–77
3. Moure C, Peña O. Recent advances in perovskites: Processing and properties. *Progress in Solid State Chemistry*; 43(4):123–48.
4. Ashim Kumar Bain, Chand P. *Ferroelectrics* [Internet]. John Wiley & Sons; 2017 [cited 2023 May 1]. Available from: <https://www.wiley.com/en-ie/Ferroelectrics:+Principles+and+Applications-p-9783527342143>
5. F. A. R. A. Jowder and Boon-Teck Ooi, "Series compensation of radial power system by a combination of SSSC and dielectric capacitors," in *IEEE Transactions on Power Delivery*, vol. 20, no. 1, pp. 458-465, Jan. 2005, doi: 10.1109/TPWRD.2004.837110
6. Ashim Kumar Bain, Chand P. *Ferroelectrics* [Internet]. John Wiley & Sons; 2017 [cited 2023 May 1]. Available from: <https://www.wiley.com/en-ie/Ferroelectrics:+Principles+and+Applications-p-9783527342143>
7. Haertling GH. Ferroelectric ceramics: history and technology. *Journal of the American Ceramic Society*. 1999 Apr;82(4):797-818.
8. Moure C, Peña O. Recent advances in perovskites: Processing and properties. *Progress in Solid State Chemistry* [Internet]. 2015 Dec 1 [cited 2023 Apr 23];43(4):123–48. Available from: <https://www.sciencedirect.com/science/article/pii/S0079678615000230#fig3>
9. Haertling GH. Ferroelectric ceramics: history and technology. *Journal of the American Ceramic Society*. 1999 Apr;82(4):797-818.
10. Zeb A, Milne S. This is a repository copy of High temperature dielectric ceramics: a review of temperature-stable high-permittivity perovskites. *High Temperature Dielectric Ceramics: a review of temperature-stable high-permittivity perovskites* [Internet]. [cited 2023 Apr 25]. Available from: <https://core.ac.uk/download/pdf/42617993.pdf>
11. Hu Z, Koval V, Yue Y, Zhang M, Jia C, Abrahams I, et al. Structural evolution and coexistence of ferroelectricity and antiferromagnetism in Fe, Nb co-doped BaTiO₃ ceramics. *Journal of The European Ceramic Society* [Internet]. 2023 Jun 1 [cited 2023 Apr 25];43(6):2460–8. Available from: <https://www.sciencedirect.com/science/article/pii/S095522192300047X>

12. Tewatia K, Sharma A, Sharma M, Kumar A. Factors affecting morphological and electrical properties of Barium Titanate: A brief review. *Materials Today: Proceedings* [Internet]. 2021 Jan 1 [cited 2023 Apr 30]; 44:4548–56. Available from: <https://reader.elsevier.com/reader/sd/pii/S2214785320384509?token=4B3A2486BA40739F92810509695563CF7F66C90D5703347CA0007B60512616E3D67A11CC06F1BC9CE270455ADC07D7B8&originRegion=eu-west-1&originCreation=20230430140857>
13. Morrison FD, Sinclair DC, Janet, West AR. Novel Doping Mechanism for Very-High-Permittivity Barium Titanate Ceramics. *Journal of the American Ceramic Society* [Internet]. 2005 Jan 21 [cited 2023 Apr 28];81(7):1957–60. Available from: <https://ceramics.onlinelibrary.wiley.com/doi/epdf/10.1111/j.1151-2916.1998.tb02575.x>
14. Smith MB, Page K, Siegrist T, Redmond PL, Walter EC, Seshadri R, et al. Crystal Structure and the Paraelectric-to-Ferroelectric Phase Transition of Nanoscale BaTiO₃. *Journal of the American Chemical Society*. 2008 Jun;130(22):6955–63.
15. Zhao C, Huang YL, Wu J. Multifunctional barium titanate ceramics via chemical modification tuning phase structure. *InfoMat* [Internet]. 2020 Nov 1 [cited 2023 Apr 22];2(6):1163–90.
16. M Guftar Shaikh, S. Phanish, Sivakumar SM. Domain switching criteria for ferroelectrics. *Computational Materials Science* [Internet]. 2006 Aug 1 [cited 2023 May 1];37(1-2):178–86. Available from: <https://www.sciencedirect.com/science/article/abs/pii/S0927025605003757>
17. D. M. Smyth, *Ferroelectrics* 116, 117 ~1991! *Annu. Rev. Mater. Sci.* 15, 329 ~1985! M. V. Raymond and D. M. Smyth, *J. Phys. Chem. Solids* 57, 1507 (1996).
18. Wu T, Pu Y, Gao P, Liu D. Influence of Sr/Ba ratio on the energy storage properties and dielectric relaxation behaviors of strontium barium titanate ceramics. *Journal of Materials Science: Materials in Electronics* [Internet]. 2013 Jul 5 [cited 2023 Apr 30];24(10):4105–12. Available from: <https://link.springer.com/article/10.1007/s10854-013-1368-y>
19. Park CS, Chadi DJ. Microscopic study of oxygen-vacancy defects in ferroelectric perovskites. *Physical review* [Internet]. 1998 Jun 1 [cited 2023 May 1];57(22): R13961–4. Available from: <https://journals.aps.org/prb/abstract/10.1103/PhysRevB.57.R13961>
20. Vijatovic MM, Bobic JD, Stojanovic BD. History and challenges of barium titanate: Part II. *Science of Sintering*. 2008;40(3):235–44.
21. Hu Z, Koval V, Yue Y, Zhang M, Jia C, Abrahams I, et al. Structural evolution and coexistence of ferroelectricity and antiferromagnetism in Fe, Nb co-doped BaTiO₃ ceramics. *Journal of The European Ceramic Society* [Internet]. 2023 Jun 1 [cited 2023 Apr 28];43(6):2460–8. Available from: <https://www.sciencedirect.com/science/article/pii/S095522192300047X>

22. Y. Iriani, Dianisa Khoirum Sandi, None Kusumandari, Sarifah N. Investigation of Barium Strontium Titanate ($\text{Ba}_{0.95}\text{Sr}_{0.05}\text{TiO}_3$) synthesized via conventional solid-state reaction and co-precipitation route with diverse sintering temperatures. *Materials Today: Proceedings* [Internet]. 2023 Mar 1 [cited 2023 Apr 30]; Available from: <https://reader.elsevier.com/reader/sd/pii/S2214785323007733?token=7395BC4AF35789DE1B87F110154A88FBEE2C2A9EFB99B179D781CCA1DE11E9702EF0F0C66E0319EBA5FF9C3FD6CE57F1&originRegion=eu-west-1&originCreation=20230430144206>
23. Electronics in. Understanding a Ferroelectric Hysteresis Loop in Electronics [Internet]. Cadence.com. 2020 [cited 2023 Apr 29]. Available from: <https://resources.pcb.cadence.com/blog/2020-understanding-a-ferroelectric-hysteresis-loop-in-electronics>
24. Yuan, Y., Zhang, S., Zhou, X. et al. High-Temperature Capacitor Materials Based on Modified BaTiO_3 . *J. Electron. Mater.* 38, 706–710 (2009). <https://doi.org/10.1007/s11664-009-0729-z>
25. Tan Y, Viola G, Koval VV, Yu C, Mahajan A, Zhang J, et al. On the origin of grain size effects in $\text{Ba}(\text{Ti}_{0.96}\text{Sn}_{0.04})\text{O}_3$ perovskite ceramics. *Journal of The European Ceramic Society* [Internet]. 2019 Jun 1 [cited 2023 May 2];39(6):2064–75. Available from: <https://www.sciencedirect.com/science/article/pii/S0955221919300536>
26. AKTAŞ P. Synthesis and Characterization of Barium Titanate Nanopowders by Pechini Process. *Celal Bayar Üniversitesi Fen Bilimleri Dergisi*. 2020 Sep 4.
27. Forsbergh PW. Domain Structures and Phase Transitions in Barium Titanate. *Physical Review* [Internet]. 1949 Oct 15 [cited 2023 Apr 28];76(8):1187–201. Available from: <https://journals.aps.org/pr/abstract/10.1103/PhysRev.76.1187>
28. Wu T, Pu Y, Gao P, Liu D. Influence of Sr/Ba ratio on the energy storage properties and dielectric relaxation behaviors of strontium barium titanate ceramics. *Journal of Materials Science: Materials in Electronics* [Internet]. 2013 Jul 5 [cited 2023 Apr 30];24(10):4105–12. Available from: <https://link.springer.com/article/10.1007/s10854-013-1368-y>
29. Anwar S, Sagdeo PR, Lalla NP. Ferroelectric relaxor behavior in hafnium doped barium-titanate ceramic. *Solid State Communications* [Internet]. 2006 May 1 [cited 2023 Apr 29];138(7):331–6. Available from: <https://reader.elsevier.com/reader/sd/pii/S0038109806002560?token=49470491D8962746E0B05223EE578D19B46CBFDCE276D52B71B4D1E51834E5A8D21ABF573BC525E4AFE213588F821002&originRegion=eu-west-1&originCreation=20230429180720>
30. Tan Y, Viola G, Koval VV, Yu C, Mahajan A, Zhang J, et al. On the origin of grain size effects in $\text{Ba}(\text{Ti}_{0.96}\text{Sn}_{0.04})\text{O}_3$ perovskite ceramics. *Journal of The European Ceramic Society* [Internet]. 2019

Jun 1 [cited 2023 May 2];39(6):2064–75. Available from:

<https://www.sciencedirect.com/science/article/pii/S0955221919300536>

31. Mao C, Yan S, Cao S, Yao C, Cao F, Wang G, Dong X, Hu X, Yang C. Effect of grain size on phase transition, dielectric and pyroelectric properties of BST ceramics. *Journal of the European Ceramic Society*. 2014 Oct 1;34(12):2933-9.
32. Hamid Ghayour, Majid Abdellahi. A brief review of the effect of grain size variation on the electrical properties of BaTiO₃-based ceramics. *Powder Technology* [Internet]. 2016 May 1 [cited 2023 Apr 29]; 292:84–93. Available from:
<https://reader.elsevier.com/reader/sd/pii/S0032591016300286?token=C86301258B9384C0C72BE9514C576500B5F647C772FAEF994537F758A184B4A79E2086B9411FE0E817221E4E6D607CB6&originRegion=eu-west-1&originCreation=20230429214202>
33. Enhanced dielectric and piezoelectric properties of xBaZrO₃-(1-x) BaTiO₃ ceramics, L. Dong, D.S. Stone and R.S. Lakes, *J. Appl. Phys.*, 111 (2012), pp. 084107-84111
34. Sandi D, Agus Supriyanto, Anif, Jamaluddin, Yofentina Iriani. The effects of sintering temperature on dielectric constant of Barium Titanate (BaTiO₃). *IOP Conference Series: Materials Science and Engineering* [Internet]. 2016 Jan 1 [cited 2023 Apr 30]; 107:012069–9. Available from:
<https://iopscience.iop.org/article/10.1088/1757-899X/107/1/012069/meta>
35. Y. Iriani, Dianisa Khoirum Sandi, None Kusumandari, Sarifah N. Investigation of Barium Strontium Titanate (Ba_{0.95}Sr_{0.05}TiO₃) synthesized via conventional solid-state reaction and co-precipitation route with diverse sintering temperatures. *Materials Today: Proceedings* [Internet]. 2023 Mar 1 [cited 2023 Apr 30]; Available from:
<https://reader.elsevier.com/reader/sd/pii/S2214785323007733?token=7395BC4AF35789DE1B87F110154A88FBEE2C2A9EFB99B179D781CCA1DE11E9702EF0F0C66E0319EBA5FF9C3FD6CE57F1&originRegion=eu-west-1&originCreation=20230430144206>
36. Takuya Hoshina, Takizawa K, Li J, Takeshi Kasama, Hirofumi Kakemoto, Takaaki Tsurumi. Domain Size Effect on Dielectric Properties of Barium Titanate Ceramics. *Japanese Journal of Applied Physics* [Internet]. 2008 Sep 19 [cited 2023 May 1];47(9):7607–11. Available from:
<https://iopscience.iop.org/article/10.1143/JJAP.47.7607/meta>
37. Structural and dielectric properties of Zr doped BaTiO₃ synthesized by microwave assisted chemical route, M.F. Al-Hilli, *Iraqi J. Sci.*, 59 (2018), pp. 94-104